



Science Arts & Métiers (SAM)

is an open access repository that collects the work of Arts et Métiers Institute of Technology researchers and makes it freely available over the web where possible.

This is an author-deposited version published in: <https://sam.ensam.eu>
Handle ID: <http://hdl.handle.net/10985/21459>

To cite this version :

Meryeme JAMIL, Myriam DUMONT, Abdelkader BENABOU, Stephane CLENET, Jean-Claude MIPO - Application of the JMAK precipitation law in iron loss modelling to account for magnetic ageing effect - Journal of Magnetism and Magnetic Materials - Vol. 547, p.168901 - 2022

Any correspondence concerning this service should be sent to the repository

Administrator : scienceouverte@ensam.eu



Application of the JMAK precipitation law in iron loss modelling to account for magnetic ageing effect

Meryeme Jamil^a, Myriam Dumont^b, Abdelkader Benabou^{a,*}, Stéphane Clénet^a, Jean-Claude Mipo^c

^a Univ. Lille, Arts et Metiers ParisTech, Centrale Lille, HEI, EA 2697 – L2EP – Laboratoire d'Electrotechnique et d'Electronique de Puissance, F-59000 Lille, France

^b Arts & Metiers Institute of Technology; Mechanics, Surfaces and Materials Processing (MSMP), Lille, France

^c Valeo Powertrain Systems, 2 Rue André Charles Boulle, 94046 Créteil Cedex, France

ARTICLE INFO

Keywords:

Magnetic ageing
JMAK model
Iron loss model
Coercive field
Precipitation

ABSTRACT

This article deals with the modelling of iron losses due to the magnetic ageing of electrical steels used in energy conversion devices. This phenomenon is the consequence of irreversible mechanisms in the material which can be triggered by the operating temperature of electrical devices. At first, an experimental study is carried out at 180° C in order to assess the effect of isothermal ageing on electromagnetic properties of a magnetic steel sample. The results show that, during the thermal ageing, the hysteresis losses and the coercive field increase. These experimental observations, mainly caused by the formation of precipitates at the material microstructural scale, are then discussed. Considering the link between the effect of magnetic ageing on macroscopic magnetic properties (effect) and the microscopic precipitation (cause), the Johnson – Mehl – Avrami – Kolmogorov (JMAK) law describing the kinetics of precipitation was applied to model the time evolution of magnetic ageing. Once this approach was validated, it is proposed to integrate the JMAK law in the Steinmetz iron loss model.

1. Introduction

In electrical machines, ferromagnetic materials are key components for the efficiency and performance of the energy conversion process. However, in modern applications, severe operating conditions, such as thermal constraints, influence their usage properties and may induce the so-called magnetic ageing. Thus, the electrical machine performances may be significantly impacted, especially in terms of efficiency. Indeed, during the electromechanical conversion, the different sources of losses (iron losses, Joule losses) may lead to an overheating of the machine. In some applications, the temperature increases significantly, as in the case of claw pole alternators where hot spots can reach up to 180 °C. Combined with the time factor, this variation of the temperature can activate atomic diffusion and precipitation mechanisms that will modify the microstructure of the electrical steel. Thus, the macroscopic magnetic properties of the material, which are linked to the microstructure properties, will change irreversibly. This process is usually defined as the magnetic ageing [1–5]. Therefore, to predict accurately the electrical machine performances during their lifetime, it is necessary to investigate the magnetic ageing mechanisms, starting by analysing and

modelling their impact on the electromagnetic properties.

In the literature, the magnetic ageing is defined as the result of microstructural changes; in particular due to the precipitation of second phase particles (carbides and / or nitrides [6] and / or sulfurs [7]...) which act as inhibiting sites for the domain wall motion during the magnetization process by “pinning” the domain walls [8]. As a result, coercive force increases as well as the hysteresis losses. Actually, the magnetic ageing is governed by the precipitation.

On the one hand, precipitation is conditioned by different factors such as the chemical composition and the operating temperature. For example, in the case of carbide precipitation, the presence of silicon above 1% by mass content delays and can limit the precipitation of carbides [9]. Regarding carbon, its presence above the solubility limit in α ferrite facilitates its precipitation.

On the other hand, the impact of magnetic ageing depends on several parameters of the precipitates like their size, their distribution and their volume fraction [2,3,5,10]. In particular, it has been reported that the effect of precipitates becomes more significant when their average size becomes close to the thickness of the domain wall [11]. Also, in [3,5,10], based on the Néel's theory [12] of the coercive force due to inclusions,

* Corresponding author.

E-mail address: Abdelkader.Benabou@univ-lille.fr (A. Benabou).

the evolution of the coercive field is related to the volume fraction of the precipitates. Consequently, the evolution of the magnetic properties due to the magnetic ageing is directly linked to the kinetics of precipitation [4].

In the literature, various experimental studies have been carried out to help understanding the impact of magnetic ageing on magnetic properties [1,4,5,9]. However, researches have been rarely interested in modelling the time–temperature effect on the magnetic properties [2,3] and even more rarely attempted to use the causal connection between microscopic precipitation and macroscopic magnetic properties to propose a modelling approach of magnetic ageing.

Based on the relationship between macroscopic magnetic properties and microscopic precipitation parameters, it is expectable to develop a macroscopic model based on a microscopic model of precipitation kinetics to describe the evolution of the macroscopic magnetic properties during magnetic ageing, which is the aim of the present study.

The current study is composed of three sections. In Section 2, the experimental effect of an isothermal ageing at 180 °C on the magnetic properties of one low carbon low silicon steel is presented. Then, the link between the impact of magnetic ageing on the magnetic properties (coercive field and hysteresis losses) and the precipitation is underlined and analysed to better understand the relationship between the microscopic aspects and their macroscopic consequences. This analysis will clarify the kinetics and mechanisms of ageing. In Section 3, on the basis of this analysis, a first modelling attempt of the kinetics of ageing with the Johnson – Mehl – Avrami – Kolmogorov (JMAK) law is proposed. And finally, in Section 4, the JMAK law is integrated in the Steinmetz iron loss model, commonly used to determine electrical machine losses, in order to account for the effect of ageing.

2. Experimental study

2.1. Material under study

The present study was carried out on a sample extracted from a claw pole rotor made from SAE1006 steel grade. The corresponding chemical composition is presented in Table 1. In fact, by its low silicon content and its operating temperature in the machine (up to 180 °C) the studied material exhibits magnetic ageing [4]. Taking into account the geometry and dimensions of the claw pole rotor, parallelepiped samples (27 mm × 10 mm × 1 mm) were extracted by Wire Electrical Discharge Machining (Wire EDM) [13]. This cutting process has been chosen because of its low impact on the electromagnetic properties [14].

2.2. Experimental

The ageing study was carried out as presented in [4]. After an initial magnetic characterization, the sample underwent an isothermal ageing treatment at 180 °C for a total period of 69 h. At regular intervals during the heat treatment, the sample was characterized at room temperature to follow the evolution of its magnetic properties, see Fig. 1.

The magnetic measurements have been realized with a specifically developed miniaturized Single Sheet Tester (SST, see Fig. 2) to obtain the B(H) magnetic hysteresis loop [13]. The magnetic field H is measured using two high precision Hall effect probes located near the sample surface while the magnetic flux density B is determined using a secondary coil located around the sample.

Table 1
SAE1006 steel chemical composition.

	Composition (%)				
	% C	% Si	% P	% S	% Mn
% weight	<0.06%	0.07–0.6%	<0.03%	0.05%	<0.35%

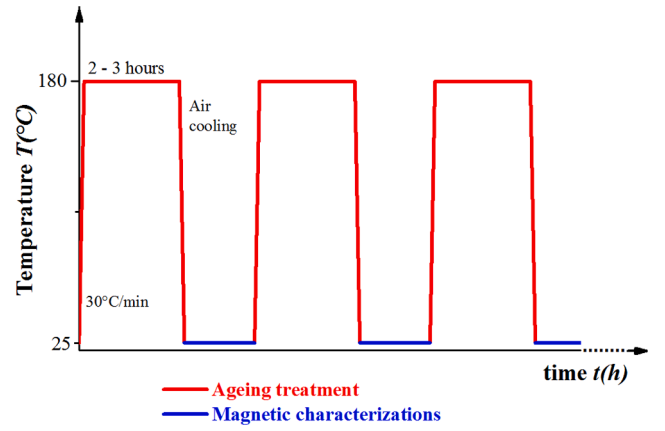


Fig. 1. Illustration of the experimental protocol.

$$B = \frac{1}{S_{smp}} \left(\frac{1}{n_2} \int v_2(t) dt - \mu_0 H S_{air} \right) \quad (1)$$

where S_{smp} is the cross section of the sample, n_2 , v_2 and S_{air} are respectively the number of turns, the voltage and the cross-section of the secondary winding, μ_0 the magnetic permeability of the vacuum and H the magnetic field estimated at the surface of the sample. The experimental device has been validated by comparison with a standard method and has a repeatability of measurements less than 2% [13].

The relevant magnetic properties are deduced from the magnetic hysteresis $B(H)$ loop presented in Fig. 3. The area of this loop is linked to the amount of energy dissipation that takes place during the magnetization process. The specific iron losses P_{tot} are then calculated from the area of the $B(H)$ loop with (Eq (2)).

$$P_{tot}(f, B) = \frac{f}{\rho} \int_{Cycle} H dB \quad (2)$$

where f is the frequency and ρ is the steel density. In the following, we will consider, as a first approach, that iron losses can be decomposed into hysteresis P_{hys} and dynamic P_{dyn} components [15] such as in (Eq (3)). Indeed, as reported in a previous study [16], the excess losses are negligible in the case of the claw pole material. Consequently, the dynamic losses are therefore limited to classical losses induced by macroscopic eddy current effects.

$$P_{tot} = P_{hys} + P_{dyn} \quad (3)$$

2.3. Experimental results

It was shown in a previous work [4] that, in the case of the studied material, the electrical conductivity σ , as well as the normal $B(H)$ curve, were not significantly impacted by the ageing treatment. Therefore, thereafter all the interest will be focused on iron losses. As mentioned above (see Eq.3), iron losses have been decomposed into hysteresis P_{hys} and dynamic P_{dyn} components. The aim of this loss decomposition is to investigate the effect of ageing on hysteresis and dynamic losses. This has been achieved by considering measurements at eight different frequencies, respectively 3, 5, 10, 20, 35, 50, 75 Hz and 100 Hz. The hysteresis losses were calculated by extrapolating the specific energy $W_{tot} = P_{tot}/f$ to zero frequency. The dynamic losses were obtained from (Eq. (3)). In Fig. 4, the respective evolutions of hysteresis losses (Fig. 4-a) and dynamic losses at 50 Hz (Fig. 4-b), for different ageing times, are presented. It is observed that the hysteresis losses are significantly affected by the ageing treatment while the dynamic losses remain unchanged. This result is corroborated by different studies [1–4]. Regarding the dynamic losses, these are mainly dependent on the electrical conductivity and magnetic flux density dynamic given by the term

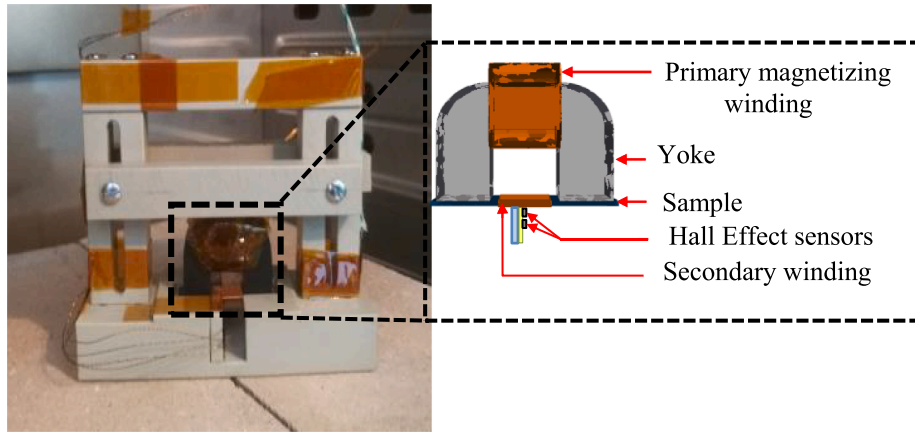


Fig. 2. Photo and illustration of the miniaturized SST for magnetic characterization.

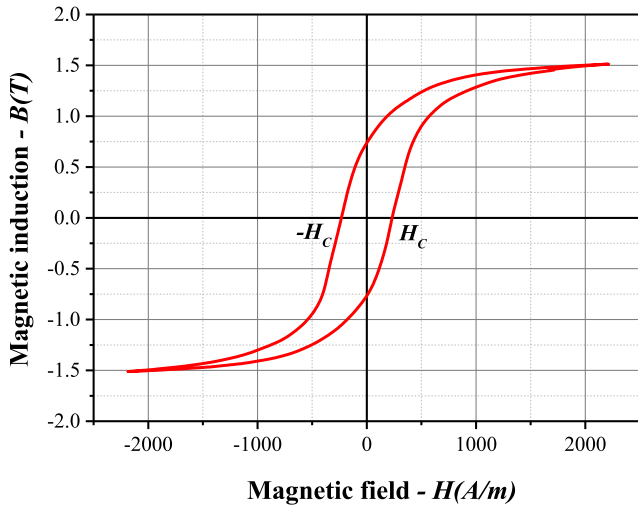


Fig. 3. Magnetic hysteresis $B(H)$ loop at 5 Hz, 1.5 T measured by a miniaturized SST.

dB/dt . This latter was verified to remain unchanged with the magnetic flux density waveform, which corroborates the results in Fig. 4-b where the dynamic losses P_{dyn} are not prone to ageing.

To describe and quantify the effect of ageing on the hysteresis losses, the ageing index AI_{hys} was calculated:

$$AI_{hys} = \frac{(P_{hys})_{after} - (P_{hys})_{before}}{(P_{hys})_{before}} \quad (4)$$

The ageing index evolution as a function of the ageing time is reported in Fig. 5. It starts to considerably increase after only few hours of heat treatment. It reaches 18% after about 25 h of thermal ageing and then tends to stabilize. The same behaviour was noted in [4] on other samples extracted from different regions of the claw pole rotor and for electrical steel laminations in [1–3].

According to the results of various studies carried out on FeSi electrical steels in [1–3] and, particularly, on the same type of samples in [4], the impact of ageing on the macroscopic magnetic properties is due to the development of microscopic precipitates. In fact, the precipitates formed during thermal treatment represent additional obstacles which hinder the movement of magnetic domain walls during the magnetization process. The precipitate / wall interaction gives rise to secondary structures known as “closure structures” in order to minimize the domain wall energy. In fact, when a domain wall meets a precipitate, a closure structure is developed around the precipitate. Then, under the pressure of the external magnetic field, the domain wall is released from the local pinning site, *i.e.* the precipitate, with additional energy dissipation. As a result, the losses increase [10]. However, it must be noted that the interaction of precipitates with domain walls depends on several

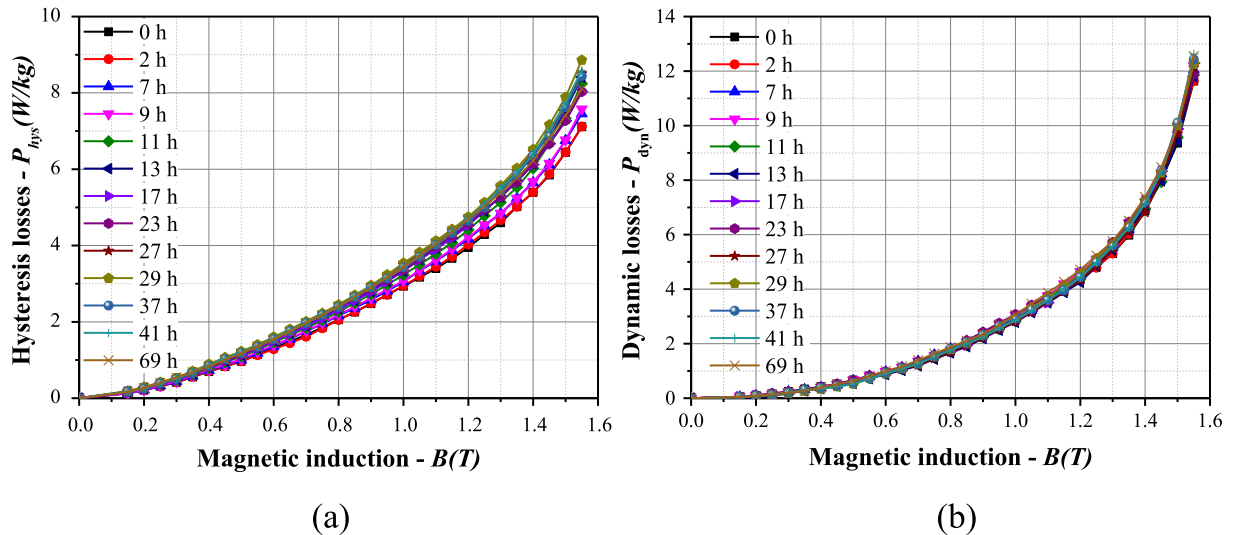


Fig. 4. (a) Hysteresis losses and (b) dynamic losses for different periods of ageing treatment at 50 Hz.

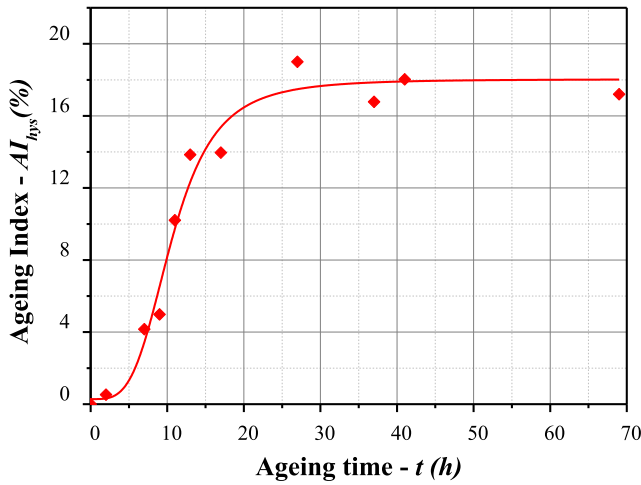


Fig. 5. Evolution as a function of the ageing time of the ageing index of the hysteresis losses (1 Hz, 1 T).

parameters; as a matter of fact, their effect is much more related to their size, volume fraction and number rather than to their nature [11].

As a consequence of this causal connection, the kinetics of ageing are linked to that of precipitation marked by three kinetic phases: nucleation, growth and coarsening. Therefore, the kinetics of ageing can be controlled by one or more of the relevant physical parameters describing these precipitates (their crystallography; their morphology; their chemical composition; their size distribution; their volume fraction; their number density and / or their magnetic character [6]). According to the literature the volume fraction and the size of the precipitates have predominant effects on the magnetic properties [2,3,5,10]. Indeed, on the one hand, it has been reported that the precipitates whose size is close to the thickness of the domain wall exhibit the greatest pinning effect hindering the displacement of the domain walls [10]. On the other hand, based on the inclusion theory of Louis Néel, the increase of the coercive field, which is an intrinsic property of the material (pointed out in Fig. 3), is proportional to the volume fraction F_v of the precipitates [3,5]. For that reason, this study investigated also the impact of magnetic ageing on the coercive field. Its evolution as a function of the ageing time presented in Fig. 6, for 1 T magnetic induction level at 1 Hz, is similar to the calculated ageing index one. It starts to considerably increase after only few hours of ageing. It increases by about 12% in less than 20 h of thermal ageing and then tends to stabilize with a variation of about $\pm 2.5\%$. The origin of this variability is partly due to the repeatability of the measuring equipment (coefficient of variation

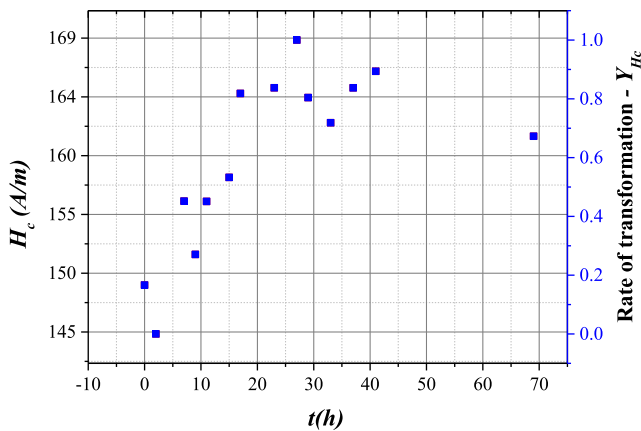


Fig. 6. Coercive field evolution as a function of thermal ageing at 180 °C and for 1 T induction level. The secondary axis gives the rate of transformation of the experimental coercive field.

$\sim 1.2\%$) and partly linked to heterogeneities in the materials like residual stresses [11] or dislocations, that may lead to variability, along with the ageing, in the coercive field H_c from one measurement to the other.

Based on this link between macroscopic magnetic properties and microscopic precipitation parameters, it is then possible to develop a model based on precipitation kinetics to describe the evolution of magnetic properties during ageing treatment.

3. Modelling of magnetic ageing

3.1. JMAK model

3.1.1. Precipitation kinetics model

Many efforts have been devoted to the modelling of precipitation kinetics in metallic alloys. Several modelling approaches have been developed in the literature at different scales: at the atomic (or nanoscopic) scale with numerical methods based on statistical physics, in particular Monte Carlo simulations [17], at the mesoscopic scale with the phase field theory [18] and at the microscopic scale [19-21]. Nano- and mesoscopic models are difficult to develop, in particular nanoscopic models because they require detailed knowledge of the interaction potentials between the different atoms that are involved in the precipitation process. For this reason, the microscopic models are considered as the most relevant scale for the present study. These models rely on equations established for the three precipitation kinetic stages. These equations are drawn from the classical theory of nucleation and the resolution of the diffusion equation (Fick's law) while accounting for the effects of interfaces (Gibbs-Thomson) during the growth and coarsening stages. They can be combined or solved numerically to give the evolution of the average characteristics of precipitation (average radius, volume fraction and density of precipitates). As a result, such models are meant to predict the precipitation kinetics as a whole. They include:

- (i) the JMAK model (Johnson-Mehl-Avrami-Kolgomorov) which only describes the evolution of the volume fraction as a function of time [19].
- (ii) the mean field model which describes the evolution of the volume fraction, the mean radius and the number of precipitates [20].
- (iii) the class model: in addition to the characteristics described by the mean-field model, the class model enables to determine the evolution of the distribution of precipitate size [21].

For the present study, and as a first approach, the JMAK model is chosen thanks to its ease of identification and limited number of required experimental data.

3.1.2. JMAK model

The JMAK model is a phenomenological model widely used to describe the kinetics of different physical phenomena, such as precipitation, phase transformation and recrystallization [22-24]. Generally, this model is employed to describe and quantify the phenomena based on the nucleation-growth process without considering coarsening. The JMAK model is established under isothermal conditions and assumes homogeneous nucleation. It does not consider grain size or even texture. Nucleation is randomly distributed in volume. It is based on the analytical equation given by:

$$Y(t) = 1 - e^{-(Kt)^n} \quad (5)$$

where $Y(t)$ is the rate of transformation. This rate corresponds to the ratio between the volume fraction of the precipitates at a given time t ($F_v(t)$) divided by the maximum volume fraction reached at equilibrium. The other parameters are n the Avrami index, which varies from ~ 1 to 4 and depends on the nucleation nature (homogeneous or heterogeneous) and precipitate morphology, and K the constant rate (in s^{-1}) [25]. This

latter depends on the number of nucleation sites and the growth rate, which itself is a function of the temperature. This parameter is expected to follow an Arrhenius law and is influenced by the diffusion coefficient.

3.2. Modelling approach of the ageing kinetic using the JMAK model

3.2.1. Application of JMAK model to the coercive field

- Model formulation

The present approach is based on inclusion theory of Néel [10] which establishes the proportionality between the coercive field and the volume fraction. Given this, the rate of transformation (the rate of variation of the coercive field due to magnetic ageing Y_{H_c}) is defined as:

$$Y_{H_c}(t) = \frac{H_c(t) - H_{cmin}}{H_{cmax} - H_{cmin}} \quad (6)$$

where $H_c(t)$ is the coercive field at a given ageing time t , H_{cmax} is the maximum value reached by the coercive field at the saturation of magnetic ageing and H_{cmin} is the minimum value of the coercive field measured before ageing. Considering that the rate Y_{H_c} is supposed to follow a JMAK law, (Eq (7)) is deduced from (Eq (5)) with the addition of the index H_c to its parameters.

$$Y_{H_c}(t) = 1 - e^{-(K_{H_c} t)^{n_{H_c}}} \quad (7)$$

- Identification of the model parameters

In order to identify the parameters (K_{H_c}, n_{H_c}), the experimental measurements of the coercive field evolution at 1 T induction level H_{c1T} , as illustrated in Fig. 6, were used. First, by applying (Eq (6)), the experimental data were converted into the rate of transformation $Y_{H_{c-exp}}$ (Eq (7)) shown in Fig. 6 with the secondary axis. Once $Y_{H_{c-exp}}$ is calculated, the JMAK parameters (K_{H_c}, n_{H_c}) are identified through a numerical fitting. In the present case, the obtained values, from the coercive field data at 1 T, are $K_{H_c} = 1.617 \times 10^{-5} \text{ s}^{-1}$ and $n_{H_c} = 1.016$. These values are comparable to those given in the literature relating to the precipitation of carbides in steels and according to which the values of n range from 1.0 to 1.5 for spherical and needle- or platelet-shaped carbide particles [26].

- Model validation

Finally, using these parameters in equation (Eq (8)), the modelled coercive field evolution $H_{cmod}(t)$ can be calculated.

$$H_{cmod}(t) = \left(1 - e^{-(K_{H_c} t)^{n_{H_c}}}\right) \Delta H_c + H_{cmin} \quad (8)$$

where H_{cmin} , $\Delta H_c = H_{cmax} - H_{cmin}$ are determined experimentally (see Fig. 6).

To check the ability of the model to predict coercive field at different induction levels, it was applied at 0.5 T, 1 T and 1.4 T. The evolution of the coercive field $H_{cmod}(t)$ obtained from the JMAK model, compared with the experimental data, is presented in Fig. 7. As it can be seen, the experimental coercive field H_c follows the prediction of the JMAK law of which parameters (K_{H_c}, n_{H_c}) were identified from the data at 1 T. This result emphasizes the ability of the JMAK model to represent the coercive field evolution and, consequently, the iron loss evolution that is detailed in the next subsection.

3.2.2. Application of JMAK model to the hysteresis losses

- Proportionality between the coercive field and the hysteresis losses

First, and according to experimental results, the hysteresis losses

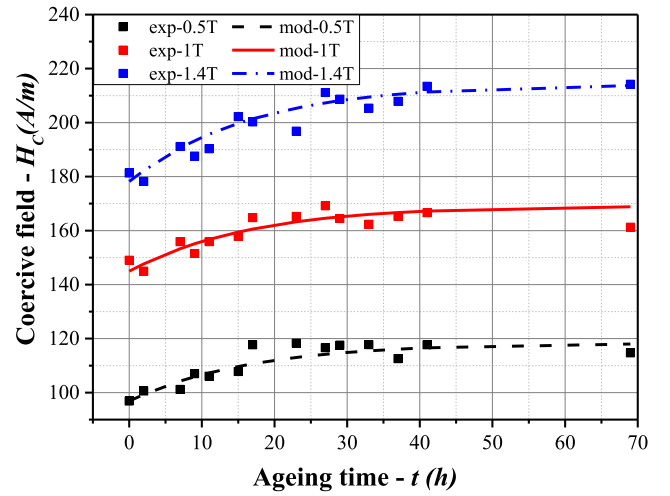


Fig. 7. Comparison between modelled coercive field and experimental measurements.

were plotted as a function of the coercive field in Fig. 8, showing a linear proportionality between both physical quantities. This result can also be sustained by relying on literature studies in [27,28], which indirectly demonstrate a proportionality, on the one hand, between the hysteresis losses and the grain size and, on the other hand, between the grain size and the coercive field.

- Application of JMAK model to the hysteresis losses

On the basis of the proportional links between the hysteresis losses P_{hys} and the coercive field H_c and between the coercive field and the volume fraction, two approaches can be distinguished to apply the JMAK law to the hysteresis losses and estimate their evolution as a function of the ageing time. The first approach consists in using the JMAK parameters identified previously for the coercive field data to assess the hysteresis losses as given by (Eq (9)).

$$P_{hysmod}(t) = \left(1 - e^{-(K_{H_c} t)^{n_{H_c}}}\right) \Delta P_{hys} + P_{hysmin} \quad (9)$$

where: $\Delta P_{hys} = P_{hysmax} - P_{hysmin}$, P_{hysmax} and P_{hysmin} are respectively the maximum value reached by the hysteresis losses due to magnetic ageing and the initial value of the hysteresis losses measured before ageing treatment.

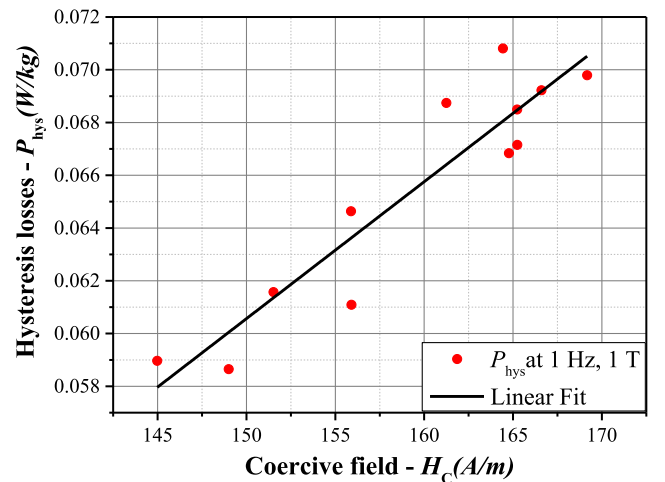


Fig. 8. Linear proportionality between the coercive field and the hysteresis losses (1 Hz, 1 T).

The second approach is the application of the same procedure of parameter identification as detailed previously in section II.2.1. The new JMAK parameters ($K_p = 1.758 \times 10^{-5} \text{ s}^{-1}$ and $n_p = 0.9173$) are then obtained by using the transformation rate of hysteresis losses $Y_{P_{hys}}$ calculated from (Eq (10)).

$$Y_{P_{hys}}(t) = \frac{P_{hys}(t) - P_{hys\min}}{P_{hys\max} - P_{hys\min}} = 1 - e^{-(K_p t)^{n_p}} \quad (10)$$

In Fig. 9 the modelled hysteresis losses were compared with the experimental measurements. The blue and black curves correspond to the modelled hysteresis losses considering, respectively, the parameters $(K, n) = (K_{H_c}, n_{H_c})$ and $(K, n) = (K_p, n_p)$. It can be observed that both results are quite close. Thus, the JMAK parameters identified from the coercive field data could be directly used to estimate the hysteresis losses, verifying also the assumption of proportionality between both physical quantities. Thereafter, the parameters identified from the coercive field data will be used because these rely directly on the Néel's theory. However, from a practical point of view, it is certainly easier to identify the JMAK parameters from the iron losses data, which allow to simplify the approach by not going through the determination of the coercive field.

Based on the presented results, it can be deduced that the proposed JMAK approach is a predictive model that, nevertheless, requires the foreknowledge of $P_{hys\min}$ and ΔP_{hys} or $H_{C\min}$ and ΔH_C which have to be determined by an experimental ageing treatment.

4. Integration of the JMAK law into the Steinmetz loss model

4.1. Steinmetz loss model

It has been shown in the previous section that we were able to model the evolution of the hysteresis losses due to magnetic ageing from the JMAK model for a given magnitude of $B = 1 \text{ T}$. To extend this possibility for any magnitude level B_{\max} , the Steinmetz model [29] as given by the equation (Eq (11)) was considered.

$$P_{hys} = C_{hys} B_{\max}^\alpha \quad (11)$$

where C_{hys} and α are parameters depending on the material. To find out which of these two parameters is the most influenced by the magnetic ageing, the experimental measurements were used to extract the model parameters (C_{hys}, α) , for each ageing time t , using a fitting procedure. Remarkably, only a slight variation of about 3% was observed on the evolution of the parameter α with the ageing time and, consequently, it

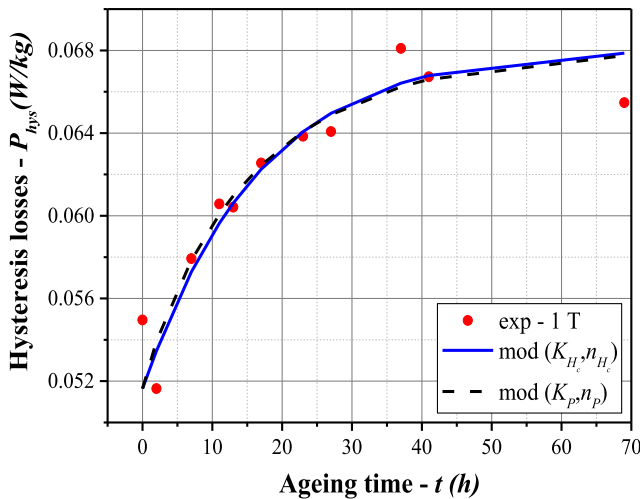


Fig. 9. Comparison between modelled hysteresis losses and experimental measurements (1 Hz, 1 T).

was considered as a constant ($\alpha = 1.55$). On the contrary, the parameter C_{hys} , which is directly linked to the hysteresis losses, varies significantly along with the ageing treatment. Its evolution, given in Fig. 10, is similar to that of the ageing index (Fig. 5).

4.2. Application of the JMAK model to the parameter C_{hys}

As the hysteresis loss coefficient C_{hys} is proportional to the hysteresis losses, it is also proportional to the volume fraction of the precipitates F_v . Consequently, the parameter C_{hys} can follow a JMAK law and can be written as in (Eq (12)).

$$C_{hys} = (1 - e^{-(Kt)^n}) \Delta C_{hys} + C_{hys\min} \quad (12)$$

where $\Delta C_{hys} = C_{hys\max} - C_{hys\min}$, $C_{hys\max}$ and $C_{hys\min}$ are respectively the maximum value reached by the hysteresis loss coefficient due to magnetic ageing and the initial value of the hysteresis loss coefficient measured before ageing treatment.

Determining the evolution of the C_{hys} coefficient from the JMAK model is an important asset as it allows to directly determine the hysteresis losses. Thus, by applying the Steinmetz model (Eq (11)) with $\alpha = 1.55$ and the C_{hys} previously calculated from (Eq (12)) using the parameters (K_{H_c}, n_{H_c}) , the evolution of the hysteresis losses as a function of the ageing time could be estimated at different frequencies and induction levels. In Fig. 11 the hysteresis losses given by the JMAK model are compared to those calculated experimentally (at 1 Hz frequency and 0.5 T, 1 T and 1.4 T induction levels).

According to the presented results, first a slight dispersion is observed on the experimental data. As discussed previously, this dispersion could have an experimental origin due to measurement errors, a numerical origin regarding the loss separation process or a physical origin due to heterogeneities in the material. Second, it was observed that the model underestimates the experimental data in Fig. 11.b and Fig. 11.c. This is mainly due to the Steinmetz model that does not fit the experimental data with the same accuracy over the whole range of induction levels. Given these considerations, the determination of the minimal and maximal values of the hysteresis loss coefficient in (Eq (12)) for a given level of induction level, can lead to some discrepancies for other levels of induction. In fact, each curve would be better fitted by a set of $P_{hys\min}$, $P_{hys\max}$ specific to each induction level. But, as a first approach, the proposed procedure consists in considering only one set of parameters $C_{hys\min}$, $C_{hys\max}$ for all the values of the magnetic induction B . Hence a greater dispersion is observed in the domains of induction level where the Steinmetz model is less accurate.

However, the global evolution of the estimated hysteresis losses by

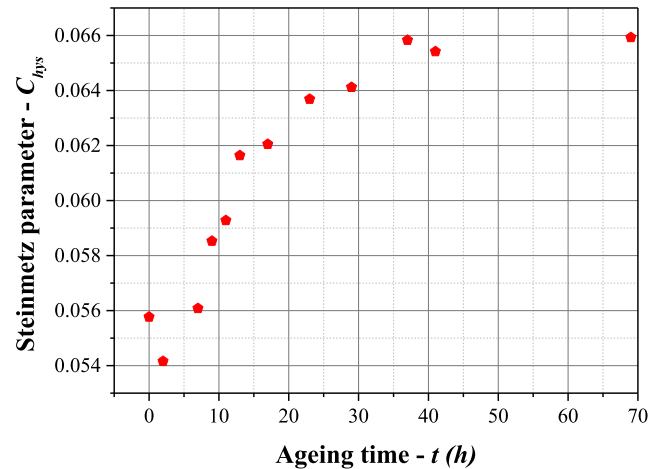


Fig. 10. Evolution of Steinmetz model parameter C_{hys} (in $\text{W.s.T}^{-\alpha} / \text{kg}$) along with the ageing treatment.

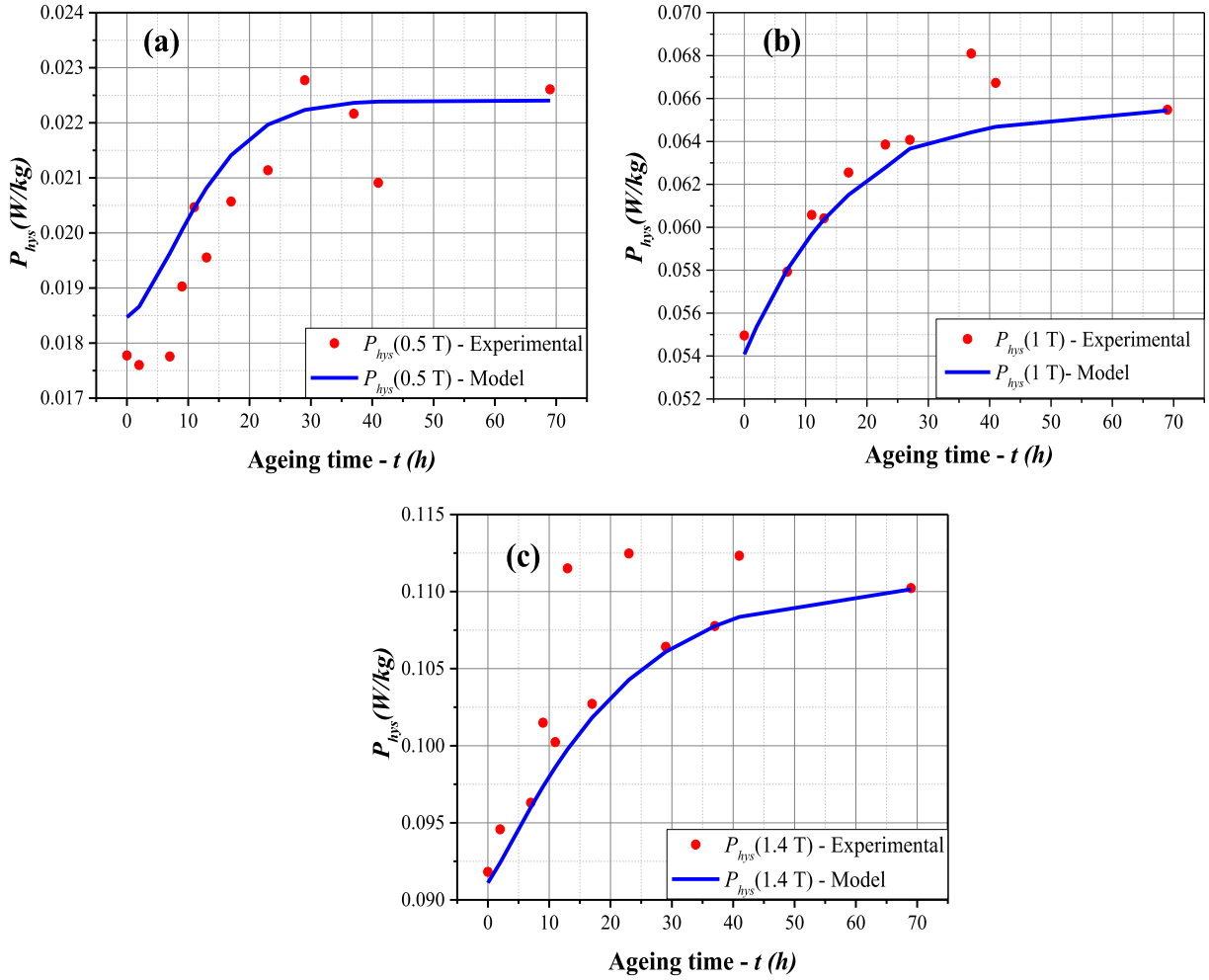


Fig. 11. Comparison between the hysteresis losses P_{hys} (1 Hz) determined from the experimental measurements and those calculated from the coefficient C_{hys} determined by the JMAK model at three induction levels (a) 0.5 T, (b) 1 T and (c) 1.4 T.

the JMAK model at different induction levels, under isothermal ageing conditions, remains in good agreement with the evolution of experimental measurements. Thus, by means of the proposed JMAK approach, the influence of magnetic ageing can be easily taken into account in the iron loss model.

4.3. Limitations of the model

At this stage of development, the proposed modelling approach requires prior determination of two constants $C_{hys,min}$ and $C_{hys,max}$ which have to be determined by a full experimental ageing treatment. Moreover, this model only considers the effect of the volume fraction of precipitates. It is however known that the size of precipitates may also alter the magnetic properties, in particular when their size is close to the thickness of domain walls. Depending on the thermal history, precipitates with various sizes may form. This physical mechanism is not accounted for by the current model. Also, in practice the operating conditions of electrical machines are not necessarily isothermal, requiring then to be able to account for temperature variations during ageing. However, considering the promising presented results, and by using the extension of the JMAK model proposed in [30], this first approach could be extended to non-isothermal conditions in order to build a generic and robust model. The parameter identification of the latter (non-isothermal model) may be realized by additional tests of accelerated ageing at higher temperature. Nevertheless, careful attention must be given to the considered temperature levels as other

microstructural mechanisms, not related to magnetic ageing, may be triggered at higher temperatures. Such study requires additional microstructural characterizations and analyses to identify the temperature range where exclusively magnetic ageing occurs.

5. Conclusion

Magnetic ageing is the consequence of microscopic mechanisms related to the diffusion and precipitation of second phase particles. Their kinetics depend on microstructural parameters such as the size and volume fraction of the precipitates. From that link between the kinetics of precipitation and the ageing effect on macroscopic magnetic properties, a preliminary modelling approach of the kinetics of ageing, in isothermal conditions, based on the JMAK law was evaluated. The application of the JMAK model to the evolution with ageing time of the main physical quantity influenced by the precipitates, i.e. the coercive field, showed very satisfactory results. Then, considering the direct link between the coercive field and the hysteresis losses that are of interest in energy conversion devices, it was proposed to integrate the proposed modelling approach into the Steinmetz loss model via the hysteresis loss coefficient C_{hys} . This approach enabled to predict the influence of magnetic ageing on iron losses under isothermal conditions. However, further developments are required to predict accurately iron losses in real conditions, especially under non-isothermal configurations. But, this preliminary study clearly proves the feasibility of developing a multi-scale model including precipitation kinetics in the determination

of iron losses in electrical machines due to magnetic ageing.

CRedit authorship contribution statement

Meryeme Jamil: Conceptualization, Methodology, Investigation, Validation, Writing – original draft. **Myriam Dumont:** Conceptualization, Methodology, Supervision, Investigation, Validation, Writing – review & editing. **Abdelkader Benabou:** Conceptualization, Methodology, Supervision, Writing – review & editing. **Stéphane Clenet:** Conceptualization, Methodology, Supervision, Writing – review & editing. **Jean-Claude Mipo:** Conceptualization, Supervision, Project administration.

Declaration of Competing Interest

The authors declare that they have no known competing financial interests or personal relationships that could have appeared to influence the work reported in this paper.

References

- [1] A.A. de Almeida, F.J.G. Landgraf, Magnetic aging, anomalous and hysteresis losses, *Mater. Res.* 22 (3) (2019), e20180506, <https://doi.org/10.1590/1980-5373-mr-2018-0506>.
- [2] J.R. de Oliveira-Júnior, et al., Kinetics of magnetic ageing of 2%Si non-oriented grain electrical steel, *Mater. Res.* 21 (1) (2018), <https://doi.org/10.1590/1980-5373-mr-2017-0575>.
- [3] G.M.R. Negri, N. Sadowski, N.J. Batistela, J.V. Leite, J.P.A. Bastos, Magnetic aging effect losses on electrical steels, *IEEE Trans. Magn.* 52 (5) (2016) 1–4, <https://doi.org/10.1109/TMAG.2016.2517942>.
- [4] M. Toto Jamil, A. Benabou, S. Clenet, S. Shihab, L. Le Bellu Arbenz, J.-C. Mipo, Magnetic ageing investigation of bulk low-carbon silicon steel, *J. Magn. Magn. Mater.* 527 (2021) 167761, <https://doi.org/10.1016/j.jmmm.2021.167761>.
- [5] M.F. de Campos, M. Emura, F.J.G. Landgraf, Consequences of magnetic aging for iron losses in electrical steels, *J. Magn. Magn. Mater.* 304 (2) (2006) e593–e595, <https://doi.org/10.1016/j.jmmm.2006.02.185>.
- [6] S.K. Ray, O.N. Mohanty, On predicting the extent of magnetic aging in electrical steels, *J. Magn. Magn. Mater.* 78 (2) (1989) 255–262, [https://doi.org/10.1016/0304-8853\(89\)90276-X](https://doi.org/10.1016/0304-8853(89)90276-X).
- [7] W.-M. Mao, P. Yang, C.-R. Li, Possible influence of sulfur content on magnetic aging behaviors of non-oriented electrical steels, *Front. Mater. Sci.* 7 (4) (2013) 413–416, <https://doi.org/10.1007/s11706-013-0219-3>.
- [8] K. Jenkins, M. Lindenmo, Precipitates in electrical steels, *J. Magn. Magn. Mater.* 320 (20) (2008) 2423–2429, <https://doi.org/10.1016/j.jmmm.2008.03.062>.
- [9] S.K. Ray, O.N. Mohanty, Magnetic ageing characteristics of low silicon electrical steels, *J. Magn. Magn. Mater.* 28 (1) (1982) 44–50, [https://doi.org/10.1016/0304-8853\(82\)90027-0](https://doi.org/10.1016/0304-8853(82)90027-0).
- [10] L.J. Dijkstra, C. Wert, Effect of inclusions on coercive force of iron, *Phys. Rev.* 79 (6) (1950) 979–985, <https://doi.org/10.1103/PhysRev.79.979>.
- [11] J. Wang, Q. Ren, Y. Luo, L. Zhang, Effect of non-metallic precipitates and grain size on core loss of non-oriented electrical silicon steels, *J. Magn. Magn. Mater.* 451 (2018) 454–462, <https://doi.org/10.1016/j.jmmm.2017.11.072>.
- [12] M.L. Néel, Nouvelle théorie du champ coercitif, *Physica* 15 (1–2) (1949) 225–234.
- [13] M. Jamil, A. Benabou, S. Clenet, L. Arbenz, J.-C. Mipo, Development and validation of an electrical and magnetic characterization device for massive parallelepiped specimen, *Int. J. Appl. Electromagn. Mech.* (2019) S1–S8, <https://doi.org/10.3233/JAE-191491>.
- [14] H. Naumoski, B. Riedmüller, A. Minkow, U. Herr, Investigation of the influence of different cutting procedures on the global and local magnetic properties of non-oriented electrical steel, *J. Magn. Magn. Mater.* 392 (2015) 126–133, <https://doi.org/10.1016/j.jmmm.2015.05.031>.
- [15] A. Krings, J. Soulard, Overview and comparison of iron loss models for electrical machines, *J. Electr. Eng.* 10 (3) (2010) 8.
- [16] M. Toto Jamil, A. Benabou, S. Clenet, S. Shihab, L. Le Bellu Arbenz, J.-C. Mipo, Magneto-thermal characterization of bulk forged magnetic steel used in claw pole machine, *J. Magn. Magn. Mater.* 502 (2020) 166526, <https://doi.org/10.1016/j.jmmm.2020.166526>.
- [17] F. Soisson, G. Martin, Monte Carlo simulations of the decomposition of metastable solid solutions: transient and steady-state nucleation kinetics, *Phys. Rev. B* 62 (1) (2000) 203–214, <https://doi.org/10.1103/PhysRevB.62.203>.
- [18] H. Shercliff, M. Ashby, A process model for age hardening of aluminium alloys—II. Applications of the model, *Acta Metall. Mater.* 38 (10) (1990) 1803–1812.
- [19] M. Fanfoni, M. Tomellini, The Johnson-Mehl-Avrami-Kohnogorov model: a brief review, *Il Nuovo Cimento D* 20 (7) (1998) 1171–1182, <https://doi.org/10.1007/BF03185527>.
- [20] M. Perez, A. Deschamps, Microscopic modelling of simultaneous two-phase precipitation: application to carbide precipitation in low-carbon steels, *Mater. Sci. Eng.* 360 (1–2) (2003) 214–219.
- [21] M. Perez, M. Dumont, D. Acevedo-Reyes, Implementation of classical nucleation and growth theories for precipitation, *Acta Mater.* 56 (9) (2008) 2119–2132, <https://doi.org/10.1016/j.actamat.2007.12.050>.
- [22] W.A. Johnson, R.F. Mehl, Reaction kinetics in processes of nucleation and growth, *Trans. Am. Inst. Min. Metall. Eng.* 135 (1939) 416–441.
- [23] M. Avrami, Kinetics of phase change. I General theory, *J. Chem. Phys.* 7 (12) (1939) 1103–1112.
- [24] A.N. Kolmogorov, On the statistical theory of the crystallization of metals, *Bull. Acad. Sci. USSR, Math. Ser.* 1 (3) (1937) 355–359.
- [25] J.W. Christian, *The Theory of Transformations in Metals and Alloys*, third Revised ed., Pergamon, 2002.
- [26] A. Zhu, S.I. Neife, E. Pink, Characterization of medium- and low-temperature carbides in a low-carbon steel by internal friction, *Steel Res.* 67 (11) (1996) 507–512, [https://doi.org/10.1002/\(ISSN\)1869-344Xa10.1002/srin.1996.67.issue-1110.1002/srin.199605528](https://doi.org/10.1002/(ISSN)1869-344Xa10.1002/srin.1996.67.issue-1110.1002/srin.199605528).
- [27] G. Bertotti, Direct relation between hysteresis and dynamic losses in soft magnetic materials, *J. Phys. Colloq.* 46 (C6) (1985) C6–389.
- [28] F.J.G. Landgraf, J.R.F. da Silva, D. Rodrigues Jr., Determining the effect of grain size and maximum induction upon coercive field of electrical steels, *J. Magn. Magn. Mater.* 323 (18) (2011) 2335–2339, <https://doi.org/10.1016/j.jmmm.2011.03.034>.
- [29] C.P. Steinmetz, On the law of hysteresis, *Proc. IEEE* 72 (2) (1984) 197–221.
- [30] A.R. Massih, L.O. Jernkvist, Transformation kinetics of alloys under non-isothermal conditions, *Model. Simul. Mater. Sci. Eng.* 17 (5) (2009), 055002.